Suitability study of Endless Strip Production technology for fabrication of API grades

A. Smith, M. Lubrano, A. Di Schino, A. Guindani

Production of hot rolled strip for oil and gas transport pipelines requires a fine and homogeneous microstructure and careful choice of chemical composition in order to meet strength, toughness, and weldability requirements. Whilst hot rolled coils to grade X80, produced by conventional continuous casting and hot rolling, are a commercial reality, there is great interest in producing API grades manufactured by the alternative (and more economical) thin slab direct rolling route.

The current work has assessed the feasibility of producing hot rolled strip of grades X65-X70 using the endless strip production layout (ESP), originally developed at Arvedi. The study was carried out using a metallurgical modelling system based on empirical equations describing austenite evolution, transformation and mechanical properties. Using this approach it was possible to study the effects of initial slab thickness, reduction ratio and chemical composition on the mechanical properties of strips in a thickness range of 10 to 20 mm. In this way, for each grade, the optimum rolling schedules, microstructures and chemical compositions could be obtained.

Keywords: Thin slab direct rolling - Endless strip production - API grades, X65, X70 - Metallurgical Modelling - Austenite Evolution.

INTRODUCTION

Production of API grades via the thin slab direct rolling (TSDR) route presents several metallurgical challenges which must be overcome to meet the required mechanical properties. These challenges include:

- At the entrance to the hot rolling mill, the austenite microstructure is an inhomogeneous as-cast structure, containing a mixture of columnar and equiaxed grains. Mean grain sizes range from 650 to 1000 µm [1]. In addition, the total rolling reduction in the TSDR process is limited (initial slab thickness typically 80 mm), compared with conventional hot rolling (200 to 250 mm slab thickness [1,2]). These two issues can give rise to a final strip having a coarse and non-uniform microstructure with also hard constituents present [3]. The mechanical properties may thus be impaired i.e. reduced strength and toughness.

A. Smith, M. Lubrano, A. Di Schino
Centro Sviluppo Materiali S.pA., Italy

A. Guindani
Acciaieria Arvedi S.p.A.

Paper presented at the Int. Conf. ROLLING 2013, Venice 10-12 June 2013, organized by AIM

- During the TSDR process, there is a significant risk of longitudinal cracking occurring during casting, if working is performed in the hypoperitectic range (0.09 wt% to 0.17 wt% carbon content) [4]. This places extra limits on the steel chemical composition that can be used.

Considering these issues, it is clear that the production of API grades with TSDR technology requires careful design of steel chemistry and rolling schedule, to produce strips having the desired properties.

This study has been performed to assess the feasibility of producing API grades X60 to X70 using TSDR technology, focusing on the Arvedi ESP mill [5] as an example. The approach was to use a modelling system developed at Centro Sviluppo Materiali (CSM), which incorporates temperature evolution during hot rolling, rolling mill parameter calculation, microstructure evolution, and finally mechanical property prediction for the hot rolled strip. Using this model system, the optimum rolling schedules, microstructures and chemical compositions could be obtained for each API grade, also identifying the coil thickness range achievable.

INITIAL DESIGN OF CHEMICAL COMPOSITION AND ROLLING SCHEDULES

For the modelling approach used, it was first necessary

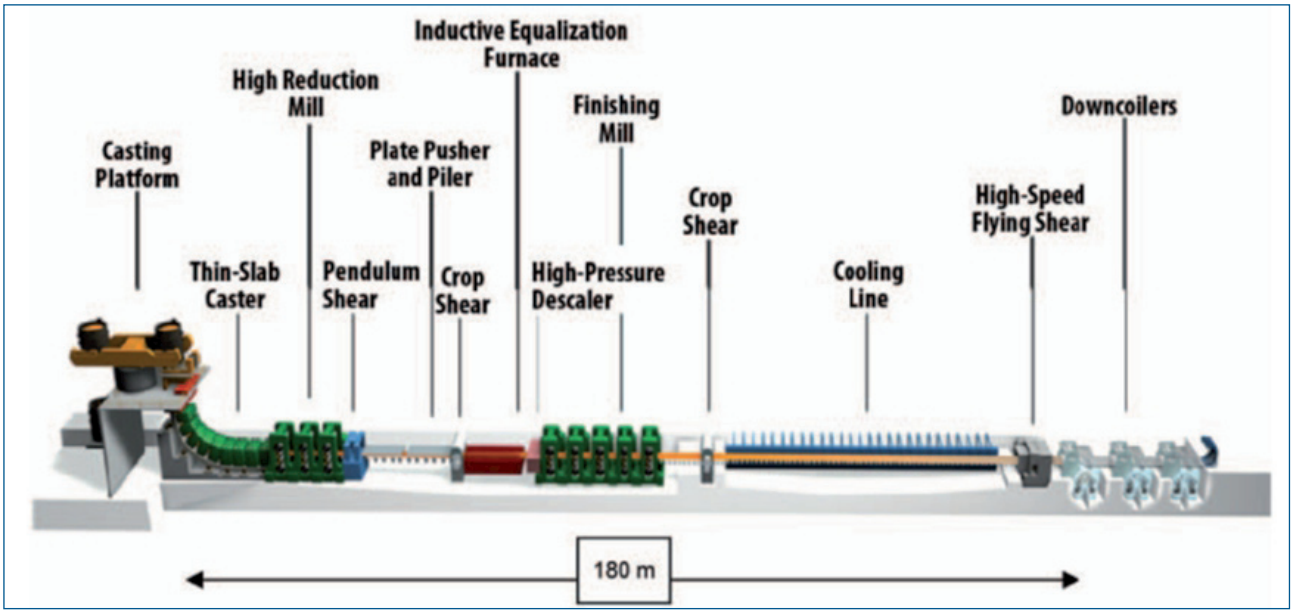

Fig. 1 - Arvedi ESP line layout [5].

Fig.1 - Layout della linea ESP in Arvedi [5].

to design an initial steel composition, suitable for pipeline grades X65 and X70. The following criteria were used:

- Composition to be suitable for pipeline grades X65 and X70, as specified in API 5L [6].
- Avoid carbon contents in the range 0.09 to 0.17 wt% so that longitudinal cracking during casting does not occur [4].
- Select an initial, C, Mn, and Nb level typical of above grades, for confrontation with ESP mill rolling force limits.

For the second point it has been suggested that to avoid solidification in the peritectic range and therefore longitudinal cracking, the carbon equivalent (C_{eq-p}) as defined below, should be less than 0.1 wt% [7]:

$$C_{eq-p} = [C] + 0.014[Mn] + 0.023[Ni] - 0.037[Si] - 0.222[S] - 0.04[P] + 0.003[Cu] - 0.004[Mo] \quad (1)$$

Where element amounts are the total ones present in the steel.

Considering the above points, the following steel was selected as the initial chemical composition:

- 0.06C-1.5Mn-0.2Si-0.06Nb.

Using this composition, suitable rolling schedules have been designed using the layout of the Arvedi ESP mill as shown schematically in figure 1.

As can be seen from figure 1, after casting, roughing is performed in 3 stands (high reduction mill), followed by heating of the transfer bar in an induction furnace. Next finishing is performed in 5 stands, with the option of inter-stand water cooling. Finally the strip reaches the run-out table (cooling line) where rapid water jet cooling is employed, followed by coiling of the strip (down coilers).

For the rolling schedule optimisation (thermal and mechanical parameters), the following requirements were respected:

- Final strip thickness values of 10 mm, 15 mm and 20 mm. This range was chosen as it corresponds to thickness values relevant for spiral welded pipe.
- Initial slab width of 1500 mm.
- Rolling force and motor power not to exceed ESP mill capabilities (considering also initial chemical composition chosen previously).
- Last finishing pass above, but close to austenite to ferrite transformation temperature (Ar_3).
- Reduction per pass during roughing above 10% to reduce chance of partial recrystallization.
- Maximum casting speed controlled to allow time for slab solidification before roughing.

Using the above requirements, rolling schedules were simulated using a thermal mechanical model having the following salient features:

- Temperature prediction in slab/strip thickness achieved using 1D finite-difference approach.
- Rolling force and motor power predicted using steel composition, based on database of flow stress data measured at ESP plant.

Simulations were performed varying the initial slab thickness (80 mm and 120 mm investigated), and the transfer bar thickness (i.e. that after roughing, 3 values chosen). For a particular final strip thickness, these two variables have a strong influence on the mechanical properties since the amount of grain refinement depends on the total reduction available i.e. initial slab thickness, and also on the amount of reduction in finishing i.e. related to transfer bar thickness. Figure 2 shows example

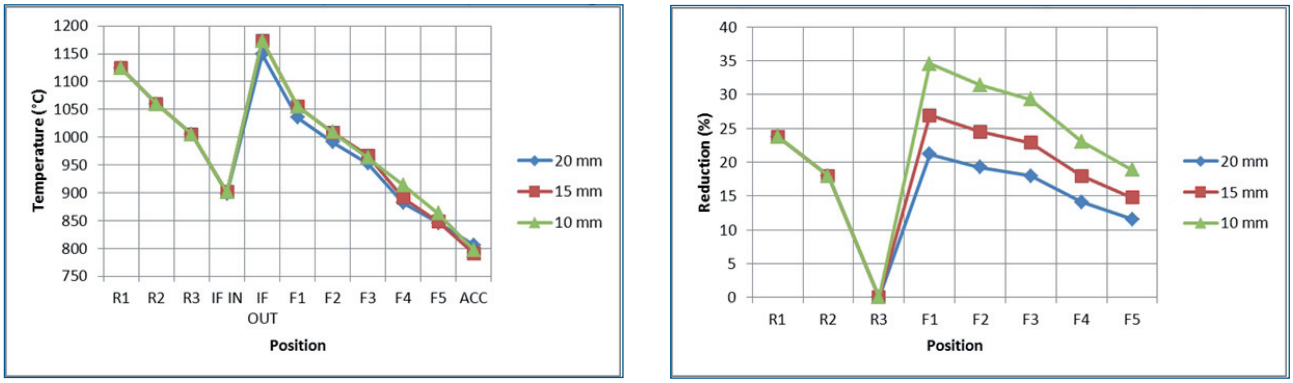

Fig. 2 - Evolution of average slab/strip temperature and rolling reduction for 80-50-X schedules. A) Temperature evolution. B) Rolling reductions. Note positions for roughing (R1-R3), entrance/exit induction furnace (IF IN/OUT), finishing (F1-F5), and entrance to cooling line (ACC).

Fig. 2 - Evoluzione della temperature media e dei tassi di riduzione. A) Evoluzione della temperatura. B) Tassi di riduzione.

simulation results (temperature and rolling reduction), whilst table 1 summarises the optimised rolling schedules obtained.

From figure 2A, the average slab/strip temperature is that at the entrance to each position shown. It can be seen that roughing starts at around 1125°C, whilst finishing starts at around 1050°C. This finishing temperature is controlled by use of the induction furnace, e.g. in the example of figure 2A, the furnace heats the transfer bar rapidly from around 900°C to about 1175°C. After finishing, the strip reaches the accelerated cooling plant entrance with a temperature of around 800°C, which is above the Ar_3 temperature for the initial steel composition studied (785°C). Figure 2B reveals that for the 80-50-X series of schedules (X is the final strip thickness of 10 mm 15 mm or 20 mm), the third rolling stand was not needed to produce the desired final strips.

From table 1 it can be seen that for the 80 mm slab case, transfer bar thicknesses of 33 mm to 50 mm were demonstrated as feasible, corresponding to a transfer bar ratio (transfer bar thickness/final strip thickness) of 1.65 to 5.00. For the 120 mm slab, transfer bar thickness values of 50 mm to 75 mm were obtained i.e. giving transfer bar ratios of 2.50 to 7.50. For the casting speed, generally higher values are favoured from a productivity point of view. For 80 mm slabs 5.5 m/min was considered the maximum feasible. For 120 mm slabs, the optimum casting speed was found to be 3.5 m/min, with higher values not giving enough time for solidification before roughing started.

Schedule No.	Initial slab thickness (mm)	Transfer bar thickness (mm)	Final strip thickness (mm)	Casting speed (m/min)
1	80	33	20	5.5
2	80	33	15	5.5
3	80	33	10	5.5
4	80	40	20	5.5
5	80	40	15	5.5
6	80	40	10	5.5
7	80	50	20	5.5
8	80	50	15	5.5
9	80	50	10	5.5
10	120	50	20	3.5
11	120	50	15	3.5
12	120	50	10	3.5
13	120	60	20	3.5
14	120	60	15	3.5
15	120	60	10	3.5
16	120	75	20	3.5
17	120	75	15	3.5
18	120	75	10	3.5

Tab. 1 - Designed rolling schedules based on ESP layout for production of hot rolled strips with 10 mm, 15 mm and 20 mm thickness.

Tab. 1 - Schede di laminazione per layout ESP per la produzione di nastri di 10, 15 e 20 mm di spessore.

MODEL FOR MICROSTRUCTURE EVOLUTION AND MECHANICAL PROPERTIES

The metallurgical modelling approach used for this study consists of an austenite evolution module, a transformation module, and a mechanical properties module. For the austenite module, the initial condition assumed is a uniform austenite structure characterised by a grain size of 1000 µm. Although a distribution of grain sizes was not modelled, it is expected that the choice of 1000 µm will be reasonably conservative. Starting from this initial condition, the austenite evolution from the entrance of the first roughing stand (R1) to the entrance of the cooling line (ACC), is simulated considering the following phenomena:

- Recrystallization kinetics.
- Recrystallized grain size.
- Grain growth after recrystallization.
- Strain induced precipitation of Nb(C,N).

Phenomenon	Equations and numbers	References
Transition strain ε_T between SRX and MDRX	$\varepsilon_T = 1.7\varepsilon_p$ (2)	[8-10]
Peak strain ε_p	$\varepsilon_p = \left[\frac{1+20[Nb]}{1.78}\right] 2.8\times10^{-4} D_0^{0.5} \left[\dot{\varepsilon} exp\left(\frac{375000}{RT}\right)\right]^{0.17}$ (3)	[11]
SRX kinetics i.e. fraction recrystallized X_{SRX}	$X_{SRX} = 1 - exp\left(-0.693\left(\frac{t}{t_{0.5}}\right)^n\right)$ (4) $n = 28.33exp\left(\frac{-36000}{RT}\right)$ (5) $t_{0.5} = A\varepsilon^p D_0 \dot{\varepsilon}^{-0.53} exp\left(\frac{Q_{RX}}{RT}\right)$ (6) $A = 3.754\times10^{-4} exp(-7.869\times10^{-5} Q_{RX})$ (7) $p = -4.3 D_0^{-0.169}$ (8) $Q_{RX} = 148636.8 - 71981.3[C] + 56537.6[Si] + 21180[Mn] + 121243.3[Mo] + 64469.6[V] + 109731.9[Nb]^{0.5}$ (9)	[12]
SRX recrystallized grain size D_{SRX}	$D_{SRX} = 31.6\varepsilon^{-0.22} D_0^{0.42} exp\left(\frac{-22018}{RT}\right)$ (10)	CSM unpublished work
Grain size after grain growth D_{gg}	$D_{gg}^{4.5} = D_{SRX}^{4.5} + 4.1\times10^{23} t_{gg} exp\left(\frac{-435000}{RT}\right)$ (11)	[13]
Strain induced precipitation kinetics of Nb(C,N) i.e. time for 5% precipitation t_{ps}	$t_{ps} = 5.3\times10^{-7}[Nb]^{-1}\varepsilon^{-1}\left[\dot{\varepsilon} exp\left(\frac{400000}{RT}\right)\right]^{-0.5} exp\left(\frac{270000}{RT}\right) exp\left(\frac{1.3\times10^{10}}{T^3(ln(K_s))^2}\right)$ (12) $K_s = \frac{[Nb]_s[C+\frac{12}{14}N]_s}{10^{\left(2.26-\frac{6770}{T}\right)}}$ (13)	[14,15]
Total strain at each pass i, ε_{TOT}, including strain accumulation	$\varepsilon_{TOT} = \varepsilon_i + \varepsilon_{i-1}(1 - X_{i-1})$ (14)	[16]
Average austenite grain size D_i at entrance to pass i.	$D_i = D_{rex,i-1} X_{i-1}^{4/3} + D_{i-1} 1.06 exp(-\varepsilon_{i-1})(1 - X_{i-1})^{4/3}$ (15)	[17]

Table 2 - Austenite evolution model

Tab. 2 - Modello di evoluzione dell'austenite

These phenomena were described by the combination of equations/conditions indicated in table 2. Note that for recrystallization, trial simulations for the schedules in table 1 revealed that only static recrystallization (SRX) occurred i.e. metadynamic recrystallization (MDRX) was absent or not significant. For this reason, table 2 does not include an approach for this phenomenon.

An important feature of the austenite module described in table 2, is the treatment of strain induced Nb(C,N). In the simulation of each schedule, once 5% precipitation has occurred then recrystallization and grain growth are assumed to have completely stopped [16]. No further process is allowed apart from austenite deformation i.e. only strain accumulation or "pancaking" occurs in further rolling passes.

For the transformation on the cooling line, in principle several transformation products may form, depending on the cooling rate, chemical composition, and final austenite grain size. For API line pipe grades up to X70, the strength and toughness requirements may be met by ferrite + pearlite microstructures. Furthermore, for line pipe steels, the carbon content is small enough so that the pearlite fraction remains small. In this situation, the strength is dominated by the ferrite phase only i.e. the key parameter of interest becomes the ferrite grain size. The transformation module need thus only predict the ferrite grain size. The approach used is based on that in [13], with the equation modified and fitted to a database of ferrite grain sizes at CSM:

$$D_a = 1.63 C_{eq}^{-0.40} D_y^{0.45} CR^{-0.09} \quad (16)$$

Where D_a is the ferrite grain size in μm, C_{eq} is the carbon equivalent in wt%, given by $Ceq = [C] + [Mn]/6$, CR is the cooling rate during the austenite to ferrite transformation in °C/s, and D_y is the austenite grain size in μm. For the average cooling rate realised in the strip during accelerated cooling on the ESP line, values were estimated from simple empirical relations for water spray cooling, considering only the strip thickness [18]. More accurate prediction of the cooling rates were not considered necessary, since for the cooling rates expected (>5°C/s), equation (16) predicts only a very small effect of increasing cooling rate on ferrite grain size. From this empirical approach, the cooling rates obtained (at 700°C) were [18]:

- For 10 mm strip CR = 30°C/s.
- For 15 mm strip CR = 15°C/s.
- For 20 mm strip CR = 10°C/s.

For mechanical properties prediction, the yield and tensile strength are based on the equations described in [13]:

$$YS = 62.6 + 26.1[Mn]\ 60.2[Si] + 19.7(0.001 D_a)\text{-}0.5 + \sigma_{ppt} \quad (17)$$

$$UTS = 164.9 + 634.7[C] + 53.6[Mn] + 99.7[Si] + 11(0.001 D_a)^{-0.5} + \sigma_{ppt} \quad (18)$$

Where YS and UTS are in MPa, the element amounts are in wt%, the ferrite grain size is in μm, and σ_{ppt} is the precipitation hardening contribution. These precipitates are assumed to form during transformation and coiling. Relevant precipitates are assumed to be Nb(C,N) and VC. VN is not considered as N is expected to be bound in Nb precipitates. To estimate σ_{ppt} for Nb precipitates, a value of 1500 MPa per wt% of total Nb content was used [19,20]. This value represents the "practical" hardening expected for Nb precipitates in ferrite, considering that some fraction of the total Nb will be unavailable, having previously precipitated in austenite. For VC precipitates a value of 500 MPa per wt% of total V is used [19]. The total estimate for precipitation strengthening is then given by:

$$\sigma_{ppt} = 1500[Nb]_{TOT} + 500[V]_{TOT} \quad (19)$$

Concerning toughness, the relevant parameter is the 50% Charpy fracture appearance transition temperature (FATT), i.e. the temperature at which the fracture surface of a Charpy impact specimen is 50% brittle. This fracture appearance transition temperature is given by the equation below, based on references [21] and [22]

$$50\%FATT = 19 + 44[Si] + 2.2(\%Pearlite) - 11.5(0.001D_a)^{-0.5} + 0.4\sigma_{ppt} \quad (20)$$

Where σ_{ppt} is that from equation (19), and the amount of pearlite is estimated using the iron-carbon phase diagram.

RESULTS OF AUSTENITE EVOLUTION MODELLING

The austenite evolution was modelled for each schedule in table 1, using the model in table 2, together with an initial austenite grain size of 1000 μm. For the chemical composition, starting from that indicated in section 1, simulations were performed tuning the Nb level for each schedule, so as to obtain the maximum amount of pancaking in finishing, whilst avoiding strain induced precipitation in roughing. The level of N was maintained at 0.004 wt% in all cases as a typical value, whilst V was not included at this stage of the modelling exercise (the effect of vanadium was found to be very small in the hot rolling stage).

The general results of the simulations in terms of the average austenite grain size and fraction recrystallized, are shown by the examples in figure 3. Note that for clarity, the grain size at the entrance to R1 (1000 μm), and refined value at R2, are not shown. Also at R3 no deformation is applied (see figure 2).

As can be seen from figure 3, during roughing, austenite recrystallizes (≥ 75%), accompanied by grain refinement. Figure 3A shows that at the entrance to finishing (F1), austenite was fully recrystallized. Inside the induction furnace recrystallization progressed and significant grain growth occurred after recrystallization was complete.

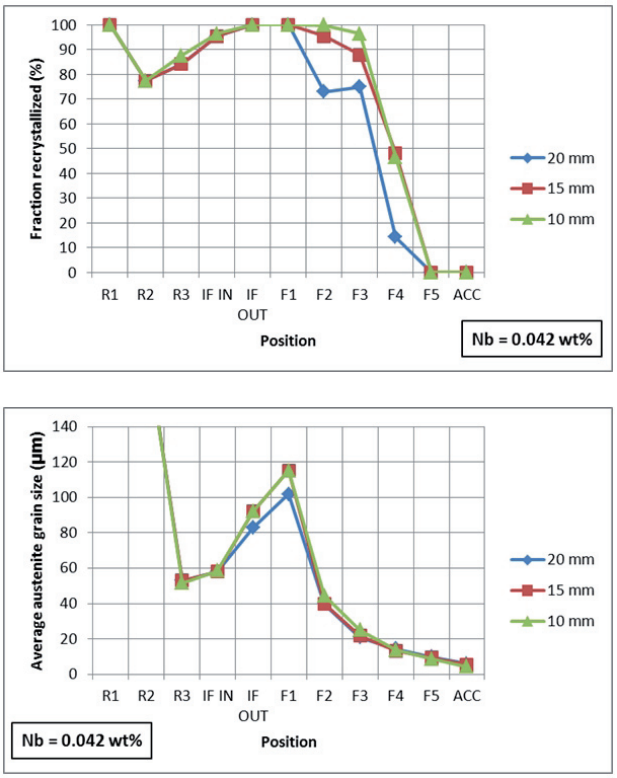

Fig. 3 - Evolution in fraction recrystallized and average austenite grain size for 80-50-X schedules. Note that values are given at the entrance to each position. A) Fraction recrystallized. B) Average austenite grain size.

Fig. 3 - Evoluzione della frazione volumetrica ricristallizzata e del grano austenitico medio per schede 80-50-X . A) Frazione volumetrica ricristallizzata. B) Grano austenitico medio.

During finishing the austenite grain size was initially refine by partial recrystallization, then by pancaking, the later due to strain induced precipitation of Nb (C,N). In the above example it was found that the maximum Nb content acceptable was 0.042 wt%, with strain induced precipitation occurring between F3 and F4 stands.

The following figures show the austenite microstructures for all simulations performed, at two critical points in the rolling mill i.e. that at the entrance to F1, and that at the entrance to the cooling line (ACC). For the former, the results are shown versus the slab ratio (initial thickness/ thickness at entrance to finishing). For the later the results are shown plotted versus the reduction in finishing i.e. the transfer bar ratio.

As can be seen from figure 4A, regardless of the level of reduction in roughing (slab ratio), the recrystallized fraction is always 100% i.e. a uniform structure is obtained before finishing starts. This homogeneous structure is obtained despite a large initial grain size (1000 μm) and even for the lowest slab ratio investigated (1.6). From figure 4B it can be seen the austenite grain size at the F1 entrance appears roughly constant as the slab ratio increases, with values in the range 94 to 141 μm. The lack of dependence

a)

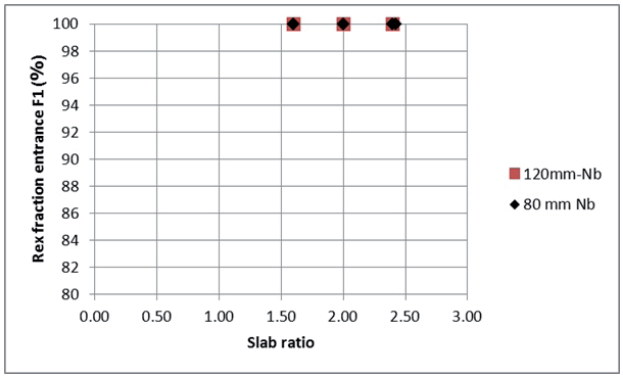

b)

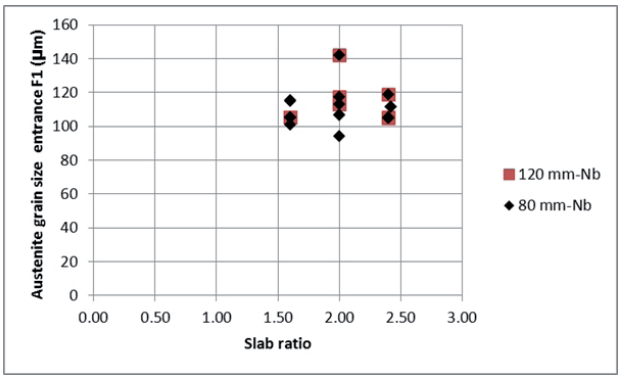

Fig. 4 - Austenite microstructure at entrance to finishing for schedules in table 1. A) Fraction recrystallized. B) Average austenite grain size.

Fig. 4 - Microstruttura dell'austenite all'entrata del finitore per le schede riportate in Tabella 1. A) Frazione volumetrica ricristallizzata. B) Grano austenitico medio.

a)

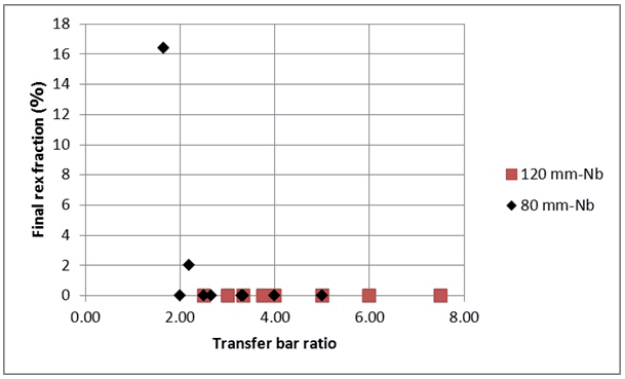

b)

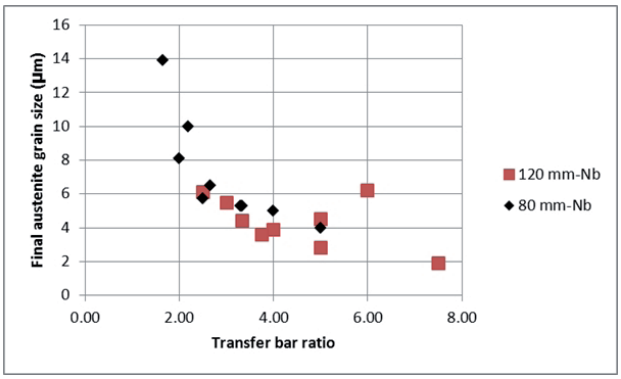

Fig. 5 - Austenite microstructure at entrance to accelerated cooling. A) Fraction recrystallized. B) Average austenite grain size.

Fig. 5 - Microstruttura dell'austenite all'ingresso del raffreddamento accelerato A) Frazione volumetrica ricristallizzata. B) Grano austenitico medio.

on slab ratio is due to grain growth between roughing and finishing, particularly inside the induction furnace.

At the entrance to accelerated cooling, figure 5A shows that as the transfer bar ratio is increased, the final recrystallization fraction quickly tends to zero. It can also be seen that to obtain a desirable uniform pancaked structure, a transfer bar ratio of at least 2.5 is needed. From figure 5B it can be seen that the average austenite grain size is generally reduced as the transfer bar ratio is increased. This is due to strain accumulation i.e. pancaking, which increases with transfer bar ratio, giving a smaller average austenite grain size – see equation (15).

Finally, concerning the Nb level optimised for each schedule, the values were found to increase slightly as transfer bar thickness increased, with values ranging between 0.034 wt% and 0.042%.

RESULTS OF MECHANICAL PROPERTIES MODELLING

For each final predicted austenite grain size, equations (16) to (20) were used to obtain the strip strength and toughness values for each schedule simulated. The results are shown in figure 6, plotted versus transfer bar ratio. Note that in all cases the steel composition was 0.06C-1.5Mn-0.2Si-0.004N-Nb, where optimised Nb values were in the range 0.034 to 0.042 wt%.

As can be seen from figures 6A and 6B, as the transfer bar ratio increases the yield and tensile strength generally increase. This is due to increasing pancaking of austenite, giving a smaller transformed ferrite grain size and hence higher strength. The effect of transfer bar ratio on toughness is illustrated by figure 6C. Again, the reduction in ferrite grain size, due to increased pancaking of austenite, is responsible for the general increase in toughness (lowering of FATT), as transfer bar ratio is increased. It is clear from these results that the amount of reduction in finishing plays a critical role in determining both strength and toughness, as far as ferrite microstructures are concerned.

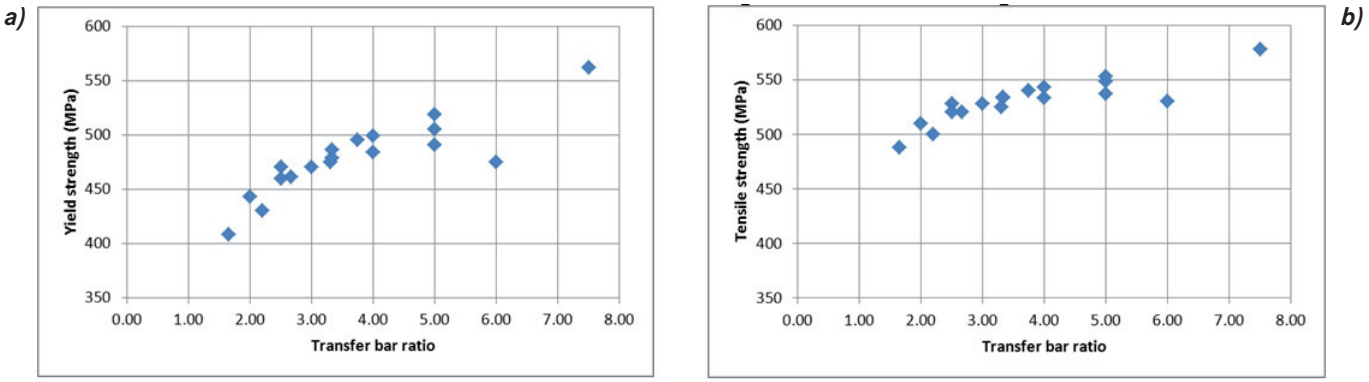

Fig. 6 - Yield strength, tensile strength, and impact toughness (FATT), for simulated schedules versus transfer bar ratio. A) Yield strength. B) Tensile strength. C) FATT.

Fig.6 - YS, UTS e 50% FATT, in funzione del rapporto di trasferimento . A) YS. B) UTS. C) 50% FATT.

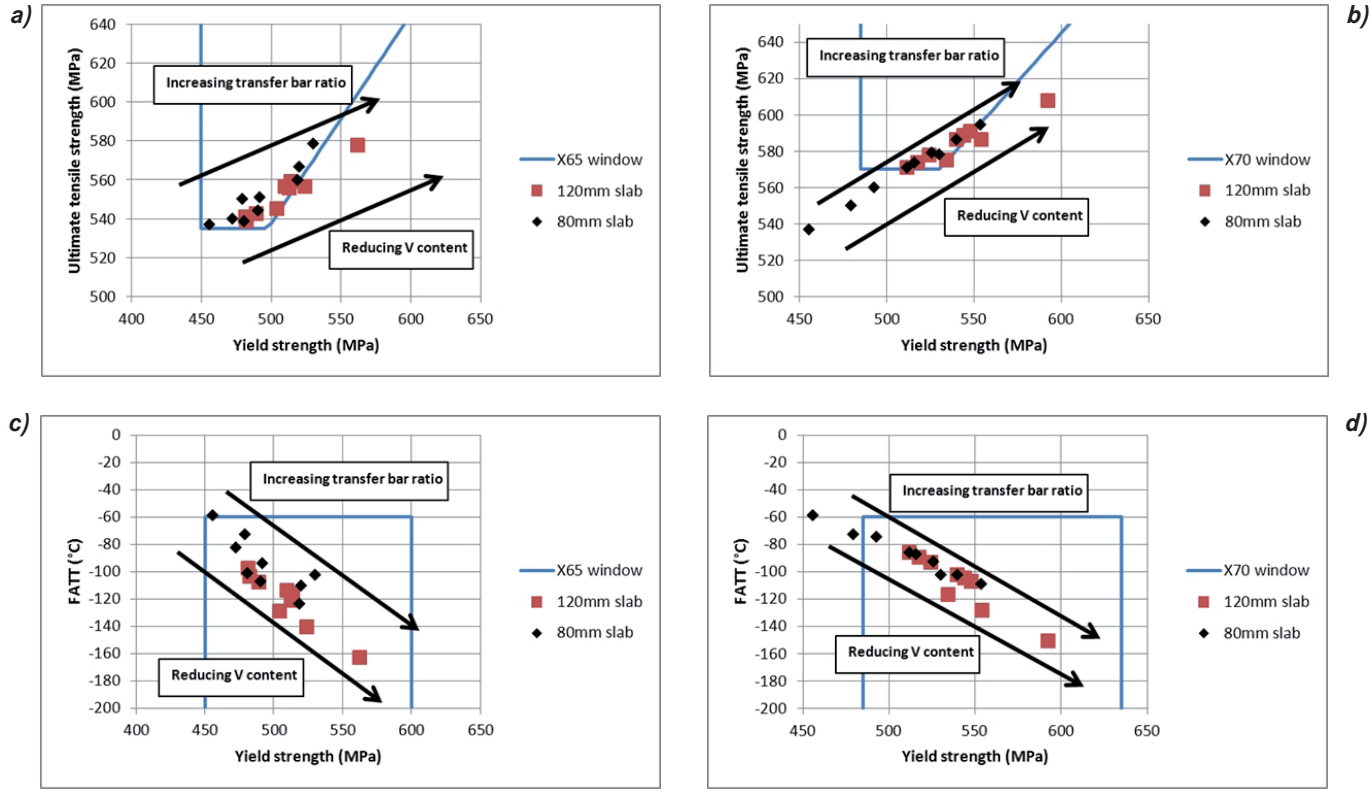

Fig. 7 - Comparison of calculated rolling schedules for optimised V and Nb additions with requirements of X65 and X70 grade line pipe steel. A) and B) Comparison with X65 and X70 strength and yield ratio requirements . C) and D) Comparison with X65 and X70 yield strength and FATT requirements.

Fig.7 - Confronto delle schede di laminazione calcolate per composizioni chimiche ottimizzate con V a d Nb (X65, X70) A)-B) Confronto con i requisiti sul carico di snervamento per X65 e X70 . C)-D) Confronto con i requisiti sul carico di snervamento e 50% FATT per X65 e X70.

OPTIMISATION OF MECHANICAL PROPERTIES FOR X65 AND X70 GRADES

For ferrite-pearlite microstructures with microalloyed precipitates, the pipeline grades X60 to X70 are in principle achievable, as long as the ferrite grain size is sufficiently refined and that precipitation hardening is optimised. From API 5L the mechanical property requirements for product specification level 2 pipe body, which has been thermomechanical rolled are given as [6]:

- X65: 450 ≤ YS (MPa) ≤ 600, 535 ≤ UTS (MPa) ≤ 760, and yield ratio ≤ 0.93.
- X70: 485 ≤ YS (MPa) ≤ 635, 570 ≤ UTS (MPa) ≤ 760, and yield ratio ≤ 0.93.

In addition, although API 5L does not specify FATT values, from CSM experience on line pipe steels, it is expected that the maximum acceptable FATT value for grades X60-X70 is -60°C.
To meet these requirements the mechanical properties for each schedule shown in figure 6, have been recalculated, with vanadium additions optimised to meet the minimum requirements for each grade. For these calculations the maximum vanadium addition considered was 0.1 wt%, based on the limits defined in API 5L. In addition the vanadium content was only optimised for transfer bar thickness. Figure 7 shows the recalculated mechanical properties for each schedule, confronted with the pipeline grade requirements defined above. Note that in all cases the steel composition was 0.06C-1.5Mn-0.2Si-0.004N-Nb-V, where optimised Nb values were in the range 0.034 to 0.042 wt% as described previously, and V levels ranged from 0 to 0.1 wt%.
For the X65 grade, figure 7A shows that for the 80 mm slab, the yield strength, tensile strength and yield ratio requirements are met for all schedules. However, from figure 7C, it can be seen that the schedule with the lowest transfer bar ratio does not meet the minimum toughness required, due to insufficient grain refinement and a large vanadium content (0.1 wt%). For the 120 mm slab, whilst toughness requirements are easily met, the yield ratio is too high for 2 of the schedules, corresponding generally to a high transfer bar ratio i.e. giving a very fine ferrite grain size.
Concerning the X70 grade, it can be seen from figure 7B for the 80 mm slab, that 3 schedules do not meet the yield and tensile strength requirements. These schedules are those with the lowest transfer bar ratio (largest ferrite grain size). In terms of toughness, one schedule for the 80 mm slab, with the lowest transfer bar ratio, fails to meet the requirement. The reason is as for the X65 case. For the 120 mm slab it can be seen that all but 2 schedules meet the tensile, yield and yield ratio requirements. These two schedules with a high transfer bar ratio give a yield ratio which is too high (very fine ferrite grain size). For the toughness requirements it can be seen from figure 7D that all schedules give acceptable FATT values.
It can also been seen from figure 7 that as transfer bar ratio is increased (decrease in ferrite grain size) the level of vanadium needed (precipitation hardening) to obtain suitable mechanical properties can be reduced. Figure 8 shows the obtained vanadium values from the optimisation exercise as a function of transfer bar thickness. Note that for each slab and transfer bar thickness, not all the final strip thicknesses met the requirements of each grade.
As can be seen from figure 8, for a fixed transfer bar thickness, the vanadium content required increases with the grade (specified minimum strength). As can be seen, for X70, very high vanadium levels are needed for all except the highest transfer bar thicknesses. For the X65 grade, a very high vanadium level is required only for the transfer bar thickness of 33 mm. In addition for the highest transfer bar ratio of 75 mm, no vanadium is required at all for the X65 grade. Finally, from an economic point of view, figure 8 clearly shows that optimisation of the rolling schedule can have significant potential cost benefits. In other words, for the X65 grade in particular, the careful control of transfer bar thickness should allow for a significant reduction in vanadium content.

CONCLUSIONS

In this study the feasibility of producing 10 mm, 15 mm, and 20 mm coils, using thin slab direct rolling technology applied to X65 and X70 line pipe grades, has been assessed via thermo mechanical and metallurgical modelling. As a basis, the Arvedi ESP technology has been used, together with appropriately designed rolling schedules and chemical compositions. From the coupled modelling of austenite evolution, phase transformation, and mechanical properties, the following conclusions may be drawn:

- The effect of Nb was to induce pancaking of austenite during finishing. For each schedule a maximum safe Nb level was identified, above which “early” strain induced precipitation would occur before finishing start. The optimum Nb content was found to be in the range 0.034 wt% to 0.042 wt%. The optimum value was also found to increase slightly as transfer bar thickness increased.
- For all schedules a uniform austenite structure (fully recrystallized) was obtained at the entrance to finishing. This was found to be the case even for the smallest slab ratio investigated (ratio of initial thickness to transfer bar thickness = 1.6).
- To obtain a uniform “pancaked” austenite microstructure at the end of finishing, the transfer bar ratio (ratio of transfer bar thickness to final strip thickness) should be at least 2.5.
- Increasing transfer bar ratio led to higher strength (YS and UTS) and greater low temperature toughness (lower FATT), through a refinement of ferrite grain size. The later was in turn due to increases strain accumulation or pancaking in austenite.
- For each schedule optimised levels of Nb and V were obtained. The required V level to meet the minimum requirements for each grade was found to reduce significantly as transfer bar thickness increased. Thus careful optimisation of transfer bar thickness may have significant cost benefits in terms of reduced V additions.
- Overall, for production of API grades X65 and X70, suitable rolling schedules have been successfully identified for coil thicknesses in the range 10 to 20 mm, for two initial slab thickness values: 80 mm and 120 mm.

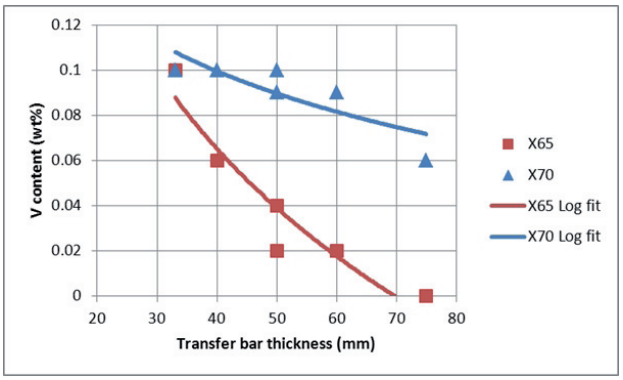

Fig. 8 - Optimised vanadium content as a function of transfer bar thickness for X65-X70 pipeline grades.

Fig. 8 - Ottimizzazione del contenuto di V in funzione del rapporto di trasferimento per X65-X70.

REFERENCES

[1] P. Uranga, B. Lopez and J. Rodriguez-Ibabe, Mater. Sci. Technol., 25, (2009), p. 1147.
[2] S. Cobo and C. Sellars, Ironmaking Steelmaking, 28, (2001), p. 230.
[3] P. Uranga, A. Fernandez, B. Lopez and J. Rodriguez-Ibabe, ISIJ Int., 44, (2004), p. 1416.
[4] P. Uranga, B. Lopez and J. Rodriguez-Ibabe, Mater. Sci. Technol., 36, (2009), p. 162.
[5] G. Arvedi, F. Mazzolari, A. Jungbauer, G. Hohenbichler, and G. Holleis, Iron Steel Technol., 8, No.7, (2011), p. 59.
[6] API specification 5L (2009), "Specification for line pipe".
[7] J. Rodriguez-Ibabe, Thin Slab Direct Rolling of Microalloyed Steels, Trans Tech Publications, Switzerland, (2007), p.79.
[8] M. Cartmill, M. R. Barnett, S. H. Zahiri and P. D. Hodgson, ISIJ Int., 45 (2005), p. 1903.
[9] P. Uranga, A. Fernandez, B. Lopez and J. Rodriguez-Ibabe, Mater. Sci. Eng. A, 345, (2003), p. 319.
[10] Z. Zhang, Y. Liu, X. Liang and Y. She, Mater. Sci. Eng. A, 474, (2008), p. 254.
[11] K. Minami, F. Siciliano, T. Maccagno, and J. Jonas, ISIJ Int., 36, (1996), p. 1507.
[12] S. Medina and A. Quispe, ISIJ Int., 41, (2001), p. 774.
[13] P. Hodgson and R. Gibbs, ISIJ Int., 32, (1992), p. 1329.
[14] R. Abad, A. Fernandez, B. Lopez and J. Rodriguez-Ibabe, ISIJ Int., 41, (2001), p. 1373.
[15] B. Dutta and C. Sellars, Mater. Sci. Technol., 3, (1987), p. 197.
[16] F. Siciliano, Jr. and J. Jonas, Metall. Mater. Trans. A, 31, (2000), p. 511.
[17] A. I. Fernandez, B. Lopez and J. M. Rodriguez-Ibabe, Scr. Mater., 46, (2002), p. 823.
[18] P. Maynier, B. Jungmann, and J. Dollet, Proc. Conf., Hardenability concepts with applications to steel, TMS-AIME, Ohio, (1978), p518.
[19] T. Baker, Mater. Sci. Technol., 25, (2009), p. 1083.
[20] H. Kejian and T. Baker, Mater. Sci. Eng. A, 169, (1993), p.53.
[21] T. Gladman, The Physical Metallurgy of Microalloyed Steels, Maney Publishing, London, (2002), p. 62-64.
[22] T. Gladman, D. Dulieu, and I. McIvor, Proc. Conf. Microalloying 75, (1975), Union Carbide Corporation, New York, N.Y. (1977), p.32.

Studio di fattibilità di gradi API attraverso tecnologia ESP

Parole chiave:

La produzione di laminati piani per tubi per trasporto di petrolio e gas richiede l'ottenimento sul laminato di una microstruttura fine ed omogenea finalizzata all'ottenimento dei requisiti in termini di proprietà tensili e di tenacità. C'è oggi grande attenzione ed interesse nel produrre laminati per tubi di grado X80 a partire da impianti di bramma sottile.
Il presente lavoro dimostra la fattibilità di nastri per tubi di grado X65-X70 attraverso tecnologia ESP, originariamente sviluppata in Arvedi. Lo studio è effettuato attraverso l'utilizzo di un modello metallurgico basato su equazioni empiriche volte a descrivere l'evoluzione dell'austenite durante il processo di laminazione, la seguente trasformazione di fase e quindi le proprietà meccaniche del prodotto finale. Seguendo tale approccio si analizza l'effetto dello spessore bramma, dei tassi di riduzione e della composizione chimica dell'acciaio sulle proprietà meccaniche di nastri con spessore nell'intervallo 10-20 mm. Lo studio permette di identificare le microstrutture e condizioni di laminazioni ottimali per i diversi gradi considerati.